Journal of Sound and Vibration (1999) **224**(5), 863–877
Article No. jsvi.1999.2165, available online at http://www.idealibrary.com on IDEAL®

AN "OPTIMAL" MODAL REDUCTION OF A SYSTEM WITH FRICTIONAL EXCITATION

R. KAPPAGANTU

Altair Engineering Inc., 1755 *Fairlane Dr, Allen Park*, *MI* 48101, *U.S.A*.

AND

B. F. FEENY

Michigan State University, *Department of Mechanical Engineering*, 2555 *Engineering Building*, *East Lansing*, *MI* 48824, *U.S.A*.

(*Received* 16 *October* 1998, *and in final form* 5 *February* 1999)

The proper orthogonal decomposition theorem is used in an "optimal" modal reduction of a frictionally excited system. The chaotic dynamics are exploited in obtaining a basis that broadly represents the system's dynamics. This basis is used in a Galerkin's approximation to reduce the system order. The reduced model is validated using qualitative and quantitative means and also from the occurrance of bifurcations. The results confirm the validity of the method and expose the benefits of using proper orthogonal modes rather than the linear natural modes of the system.

1. INTRODUCTION

Proper orthogonal decomposition (POD) is a method of spatial characterization of dynamically distributed media. POD, which will be described later as applied in the present system, yields the optimal energy distribution in a set of measured time histories of a system (Lumley [1]). POD was traced back by Lumley [1] to independent investigations by Kosambi [2], Loeve [3], Karhunen [4] and Pougachev [5]. Ravindra [6] has noted the similarity of POD with singular value decomposition (SVD), and included a discussion of the roots of SVD, as they reach back to the late 19th century, with that of Beltrami. Proper orthogonal decomposition is primarily a statistical formulation widely used in pattern recognition and image-processing communities. It is a procedure for extracting a basis for modal decomposition from an ensemble of signals. Its power lies in the mathematical properties that suggest that it is the preferred basis in many circumstances. The attractiveness of the POD lies in the fact that it is a linear procedure. The mathematical theory behind it is the spectral theory of compact, self-adjoint operators. This robustness makes it "a safe haven in the intimidating world of non-linearity; although this may not do the physical violence of linearization methods" [7]. The linear nature of the POD is the source of its

0022–460X/99/300863 + 15 $30.00/0

limitations, as will emerge from what follows. However it should be made clear that the POD involves no assumptions about the linearity of the problem to which it is applied. In this respect it is as blind as Fourier analysis [7]. The basic service of this method is to quantify the coherence in an ensemble of data. In the mechanics community, this technique was first exploited by Lumley [1] in the sixties in understanding coherent structures of turbulent flows. Until recently very few dynamicists have evinced interest in exploiting this tool for understanding the spatial distribution of energy in a dynamic system. In the recent past the POD theorem has been applied to estimate the number of active states in chaotic attractors (Cusumano *et al.* [8, 9]), model distributed systems (FitzSimons and Rui [10]), understand snap-through oscillations of buckled plates (Murphy [11]), investigate fluid structure interaction problems (Sipcic *et al.* [13]), etc., with different degrees of success. They all have used the technique in quantifying the spatial coherence of the dynamics from observed information at different locations. The foundation of this theory lies in linear concepts like coherence and this could probably be the reason for the non-linear dynamicists' hesitation in using this theory for systems showing non-linear phenomena. For lightly damped linear transient vibrations, proper orthogonal modes (POMs) converge to the linear normal modes (Feeny and Kappagantu [14]). Indeed, similarities between POMs and linear natural modes (LNMs) have been observed (Davies and Moon [15]). Generally, POMs are principal axes of the data in the measurement space. For synchronous non-linear normal modes, the dominant mode represents a best fit of the non-liner normal mode (Feeny and Kappagantu [14]). Evidence that this may carry over to multimodal non-linear responses lies in the simulation results of Ma *et al.* [16].

One is interested in looking into the feasibility of applying POD theory to systems subjected to frictional excitation and verifying the authors' hypothesis that "the proper orthogonal modes obtained from the chaotic dynamics of a higher order system subjected to frictional excitation broadly represent the system dynamics and hence can be used in building a reduced-order model for the system". The motivation comes from the fact that these systems are typical of many mechanical systems and the energy dissipation due to the resulting stick slip oscillations are known to be in the form of sound (automotive squeak, rail wheel squeal, music from a violin string, etc.) contributing to increasing maintenance costs in the automotive industry. Also, these vibrations are known to cause serious problems in high precision machining. In addition to modelling from the measured responses, POD has an added advantage that it gives the modal coupling information which is critical to understanding squeak/squeal phenomena.

Numerical and physical experiments were conducted to obtain time-series of displacements at different locations on the system where the system behavior is chaotic. This information was processed using POD theory and the dominant modes were obtained. These modes were later used in building a reduced-order model for the system. The reduced model was validated using different qualitative and quantitative comparison techniques. Systems subjected to frictional excitation were considered as a feasibility study for squeak and squeal

problems, for which one's aim would be to identify the active modes and degrees of freedom that contribute to the system dynamic response. The POD provides modes which can be used in modal reduction in place of linear natural modes which in many situations are unknown. In this paper only the numerical experiments are presented.

2. SYSTEM DESCRIPTION AND MODELLING ISSUES

The frictionally excited spring–mass–damper system depicted in Figure 1 is studied. One end of the chain is anchored. The other end mass is lying over a moving belt with only the friction force acting between the belt and the mass in the direction of oscillation. All the masses, springs and dampers are assumed identical. Proportional viscous damping is assumed. The system can be mathematically described by the equation

$$\mathbf{M}\ddot{\mathbf{X}} + c\mathbf{K}\dot{\mathbf{X}} + \mathbf{K}\mathbf{X} = \mathbf{F}, \tag{1}$$

where c is the damping coefficient, $\mathbf{M}$, $\mathbf{K}$ are the mass and stiffness matrices. The mass matrix is m times an identity matrix and the stiffness matrix is given by

$$\mathbf{K} = \begin{bmatrix} 2k & -k & \cdots & 0 & 0 \\ -k & 2k & \cdots & 0 & 0 \\ 0 & -k & \cdots & 0 & 0 \\ \vdots & \vdots & \ddots & \vdots & \vdots \\ 0 & 0 & \cdots & 2k & -k \\ 0 & 0 & \cdots & -k & k \end{bmatrix}, \tag{2}$$

where m is the mass of each block and k is the stiffness of each spring.

Noting that the friction force is acting only on the last mass, (the *driving* mass), one sees that the $\mathbf{F}$ vector in the equation (1) is all zeros except the last row. The force $\mathbf{F}$ is a column vector given by

$$\mathbf{F} = \begin{bmatrix} 0 \\ \vdots \\ 0 \\ 1 \end{bmatrix} f_\mu(\alpha, V_r, N). \tag{3}$$

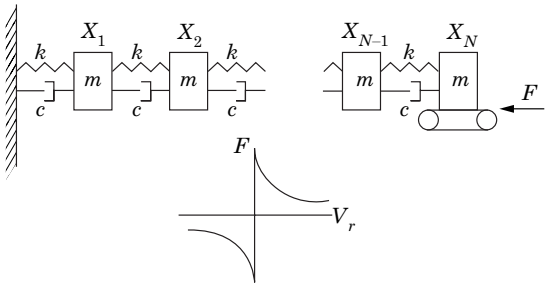

Figure 1. Configuration of spring–mass–damper system under frictional excitation.

The friction law that one used is an approximation of the Stribeck friction law and is similar to the ones used by Sugimoto [17]. When the relative velocity is not zero the friction force f_μ is the kinetic friction force and is given by

$$f_\mu = \text{sign}(V_r)(\mu_K + (\mu_S - \mu_K)\text{e}^{-\alpha|V_r|})N, \quad V_r \neq 0. \tag{4}$$

When the relative velocity is zero the friction force is the static friction force which is in dynamic equilibrium with the inertial, spring and damper forces of the system. The bounds on this static friction force are given by

$$-\mu_S N < f_\mu < +\mu_S N, \quad V_r = 0. \tag{5}$$

In the last two equations μ_K and μ_S are the kinetic and static coefficients of friction, N is the normal force between the driven mass and belt and α is a constant dependent on the properties of the contact elements.

The above set of equations is only coupled through the matrix $\mathbf{K}$ and can be solved directly by a standard numerical ODE solver, in conjunction with an algorithm that accommodates stick–slip transitions. The present algorithm is similar to that used by Whiteman and Ferri [18]. Even when the coupling is through both $\mathbf{M}$ and $\mathbf{K}$ matrices one can reduce equation (1) into a non-dimensional form. One assumes, for simplicity, m and k to be unity and the damping to be proportional and viscous. Therefore,

$$\ddot{\mathbf{X}} + c\mathbf{K}\dot{\mathbf{K}} + \mathbf{K}\mathbf{X} = \mathbf{F}. \tag{6}$$

Using the relations $Y_i = X_i$ and $Y_{i+1} = \dot{X}_i$, one can rewrite the above equations in a state-space form,

$$\dot{\mathbf{Y}} = \mathbf{A}\mathbf{Y} + \mathbf{B}f, \tag{7}$$

where the matrices $\mathbf{A}$ and $\mathbf{B}$ are

$$\mathbf{A} = \begin{bmatrix} \mathbf{0} & \mathbf{I} \\ -\mathbf{K} & -c\mathbf{K} \end{bmatrix}, \quad \mathbf{B} = \begin{bmatrix} \mathbf{0} \\ \mathbf{F} \end{bmatrix}. \tag{8, 9}$$

When the driven mass is slipping over the belt, f in the above equation represents the kinetic friction force which is known as a function of relative velocity and normal force. It is implicitly time dependent.

When the driven mass is stuck to the belt, the relative velocity is zero and the friction force that is in equilibrium with the restraining force from the springs and the inertial forces is the static friction force. One only knows that the static friction force is bounded by $(-\mu_S N, +\mu_S N)$. Also in this state, the acceleration of the driven mass would equal that of the belt $a(t)$, which in turn is zero, as the belt is considered to be moving at constant velocity. Hence,

$$0 = \dot{Y}_{2M} = \sum_{i=1}^{2M} A_{2M,i}\, y_i + B_{2M} f, \tag{10}$$

The static force f varies with time, but more specifically is dependent on the time-varying displacements of the system. Rearranging terms,

$$f = -\sum_{i=1}^{2M} A_{2M,i}\, y_i / B_{2M}. \tag{11}$$

Using this relation one can reduce the dimension of the state equation (7) by one. But for determining the slip criterion, one needs the value of the force f. Also the saving in reducing the state by one is not much considering the book keeping one has to do in the implementation of the code. As such in the implementation the authors used the full order set of equations (7) for both the stick and slip modes of the system, with f appropriately defined by equations (11) and (4) respectively.

The implementation details are as follows. The system is started with some initial conditions and the belt is moving at some speed V. From the initial conditions and the belt speed, the system mode, whether in slip or stick, is determined. The system is in the slip mode when the driving mass velocity is different from that of the belt. If the two speeds are the same, then the restraining force S on the driving mass (due to the springs, dampers and inertia) should be considered. This restraining force is in equilibrium with f, which is defined in equation (11).

If the absolute value of this force S is within the static friction force, the system is in stick mode. If it is any greater than the static friction force, the system will slip. If the system is in slip mode, the force f of equation (7) is determined by equations (4). The system is assumed to be in the slip mode. When in the slip mode the instantaneous kinetic friction force is calculated based on the relative velocity between the driving mass and the belt and this is used as an external excitation force. The integration is carried out in small time intervals Δt, until the crossover of the beltspeed by the speed of end mass (i.e., $\dot{X}_M$ crosses V). When there is a crossover, the program steps back and uses a reduced time step to calculate the state. This is continued till the end mass speed nearly equals the belt speed. At this stage, the restraining force S on the end mass is computed. If the restraining force satisfies the static force constraint, i.e., $|S| < \mu_S N$, sticking occurs. If $|S| \geqslant \mu_S N$ the system continues to slip and one continues to integrate the slip state equations.

When the system gets into the stuck mode, one integrates the state-equations corresponding to the stuck mode in small time intervals Δt and at each instant the restraining force S is calculated. This restraining force is compared with limiting static friction to check for the slipping criterion. When $|S|$ crosses $\mu_S N$, one reduces the time step and reintegrates until $|S|$ equals $\mu_S N$ within some specified tolerance. The system is then ready to slip and the slip module takes over.

To calculate the periodicity the system is run for a specified number of time steps at the end of which a check for any periodicity is made based on the slip criterion (the absolute difference between the states at successive slips is compared with the last slip recorded). In the present simulations constant belt speed is assumed. The first 1000 s of data has been discarded to account for transients. In the absence of periodicity within the 5000 s, the simulations were

continued for another 5000 s before the next check. This process was continued up to 100 000 s.

3. HIGHER ORDER DYNAMICS, CHAOS AND ITS VERIFICATION

In order to illustrate the varied dynamics of this system undergoing stick–slip oscillations, a sweep on the belt speed was carried out. Starting from a belt speed of 0·5 the belt speed was moved to 0·001 in steps of 0·001. At each belt speed the system was allowed to run until periodicity was reached or $T = 100\,000$ s, whichever is earlier. The initial conditions at each speed are set equal to the end conditions of the previous belt speed. All the displacements of the driven mass at the times of slip are recorded against the belt speed. This data is plotted with the belt speed on the x-axis and the slip displacements on the y-axis and is presented in Figure 2. At a given belt speed, n points indicate the period is n. When n is large, i.e., when there is a smear of points it indicates the dynamics are either non-periodic or the system is still in the transient stage.

Figure 2 also shows phase portraits of the driven mass with the displacement on the x-axis and velocity on the y-axis at three different belt speeds. The periodic orbits are obvious. But the non-periodic orbit needs some verification for chaos.

Phase space reconstruction studies have been used for this purpose. The Lyapunov exponents of the reconstructed attractor were determined using the algorithm of Wolf [19]. In order to minimize the effect of non-smoothness, the velocity time series of the first mass from the anchored end was used to

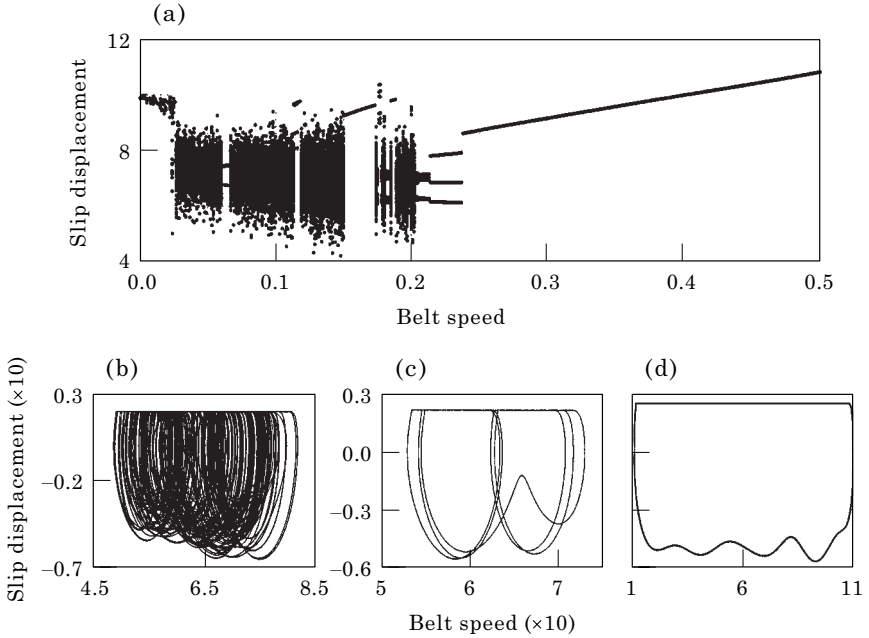

Figure 2. Bifurcation diagram of the full model (a) and a few different possible orbits (b), (c) and (d). The belt speeds for these orbits are (b) 0·20, (c) 0·22 and (d) 0·25.

reconstruct the pseudo attractor. This velocity time series was interpolated for uniform sampling. Using the first minimum of mutual information criterion [20, 21], one obtained a time delay of 11 average time periods. Using the method of false nearest neighbors [22] an embedding dimension of 6 was determined to be sufficient to unfold the attractor. With these two parameters defined one obtained the first positive Lyapunov exponent from the application of Wolf's algorithm on the time series to be 0·2833 confirming the chaotic nature of the time series.

Thus the dynamics of this frictionally excited system have been shown to become chaotic in some parameter ranges. As mentioned earlier the next step is to exploit this chaos.

4. FINDING POMS AND SYSTEM REDUCTION

The proper orthogonal decomposition theorem states that the eigenvectors of a spatial correlation matrix formed of an ensemble of data form an "optimal" basis for the ensemble. These eigenvectors are referred to as proper orthogonal modes (POMs) and the eigenvalues are known as proper orthogonal values (POVs). The POVs are proportional to the signal "energy" contained in the POMs.

In the present experiment the displacement time series of the masses form the ensemble. One collects all the displacements in a matrix $\boldsymbol{\chi}$. Each column of the matrix represents the time series of displacement of a given mass. This allows one to define the spatial correlation matrix $\mathbf{R}$ by $\mathbf{R} = \boldsymbol{\chi}^{\mathrm{T}}\boldsymbol{\chi}$. This being an Hermitian matrix of relatively small size, finding the eigenvectors is not difficult. The SVD routine of the software program MATLAB was used to do this.

The displacement data of different orbits was collected and for each of them the proper orthogonal modes determined and presented in Figure 3. Note that only those POMs that account for more than 99% of the signal energy are presented. For each of the different orbits one sees that the system shows a different set of POMs. Though for most of the cases only two modes were found to dominate and these modes happen to be the same in the limit, one does find different sets of dominant modes for different kinds of orbits. This gives rise to the problem of finding a single set of POMs that broadly represent the system.

The authors conjecture that the POMs obtained from the chaotic orbit would represent the system in the broadest sense possible. This is because of the fact that a chaotic orbit visits many unstable periodic orbits and hence should contain more information about the system than a single periodic orbit. Also, chaos has random like properties.

5. MODAL REDUCTION

5.1. THE MATHEMATICS

The dominant POMs ("dominance" criterion discussed in the next section) are represented by columns of the matrix $\mathbf{U}$. These modes are used in transforming

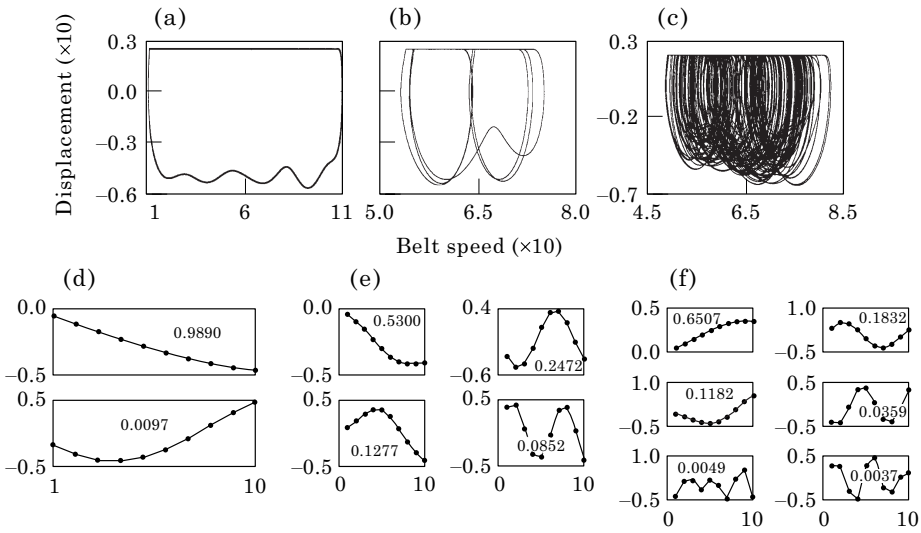

Figure 3. Typical orbits of the 10-SMD system are shown in the first row (a), (b) and (c) and corresponding dominant POMs are shown in the bottom row (d), (e) and (f). Orbits (a) and (b) are obtained at a belt speed of 0·25 with different I.C.'s and orbit (c) is obtained at a belt speed of 0·20.

the system co-ordinates $\mathbf{Y}$, to a new set of co-ordinates $\mathbf{Q}$, using the relation $\mathbf{Y} = \mathbf{VQ} + \bar{\mathbf{Y}}$, where $\mathbf{V}$ is a $2M \times 2L$ block diagonal matrix, and both the $M \times L$ blocks equal $\mathbf{U}$. $\bar{\mathbf{Y}}$ is the mean of $\mathbf{Y}$ across time. By measuring $\mathbf{Y}$ from the points of static deflection of each mass, one can easily show that $\bar{\mathbf{Y}}$ equals zero. Thus one can write $\mathbf{Y} = \mathbf{VQ}$. The usage of this transformation in the system's full model equation results in a reduced system equation. The dimension of the system equation in state space notation changes from $2M$ to $2L$ in this reduction. Here M is the number of DOF and L is the number of dominant modes. Equation (7) then leads to

$$\mathbf{V}\dot{\mathbf{Q}} = \mathbf{AVQ} + \mathbf{B}f. \tag{12}$$

Premultiplying this equation by $(\mathbf{V}^{\mathrm{T}}\mathbf{V})^{-1}\mathbf{V}^{\mathrm{T}}$ results in

$$\dot{\mathbf{Q}} = (\mathbf{V}^{\mathrm{T}}\mathbf{V})^{-1}\mathbf{V}^{\mathrm{T}}\mathbf{AVQ} + (\mathbf{V}^{\mathrm{T}}\mathbf{V})^{-1}\mathbf{V}^{\mathrm{T}}\mathbf{B}f. \tag{13}$$

Denoting $(\mathbf{V}^{\mathrm{T}}\mathbf{V})^{-1}\mathbf{V}^{\mathrm{T}}\mathbf{AV}$ by $\mathbf{A}_R$ and $(\mathbf{V}^{\mathrm{T}}\mathbf{V})^{-1}\mathbf{V}^{\mathrm{T}}\mathbf{B}$ by $\mathbf{B}_R$ one can rewrite the above equation as

$$\dot{\mathbf{Q}} = \mathbf{A}_R\mathbf{Q} + \mathbf{B}_R f. \tag{14}$$

These $2L$ equations can be integrated as before to obtain the values of Q_is at each time step. Again the definition of f is based on the slip and stick modes. As such during the slip mode one needs to constantly monitor the driven mass speed, which is given by

$$v(t) = \dot{Y}_M = Y_{2M} = \sum_{i=1}^{2L} V_{2M,i}\, Q_i \tag{15}$$

and during the stick mode define f in terms of $Q(t)$. Noting that the driven mass when stuck to the belt (moving at constant velocity) has zero acceleration, one has

$$0 = \dot{\mathbf{Y}}_{2M} = \mathbf{V}_{2M,i}\dot{\mathbf{Q}} = \mathbf{V}_{2M,i}(\mathbf{A}_R\mathbf{Q} + \mathbf{B}_R)f. \tag{16}$$

Here $\mathbf{V}_{2M,.}$ indicates the $2M$th row of the matrix $\mathbf{V}$. Moving f to the left side results in

$$f = (-1/\mathbf{V}_{2M,.}\mathbf{B}_R)\mathbf{V}_{2M,.}\mathbf{A}_R\mathbf{Q} = \mathbf{D}\mathbf{Q}, \tag{17}$$

where $\mathbf{D}$ is defined accordingly.

Noting that the POMs are obtained from experimental data, one realizes that equation (14) is a reduced order model built from experimental data, the reduction in order being from $2M$ to $2L$.

5.2. THE ORDER OF REDUCTION

Now that one knows how to construct a reduced order model, the next question is *how to decide on the order of reduction?* General practice in literature is to pick the first few modes; the sum of whose corresponding eigenvalues exceeds 99% of the sum of all eigenvalues. Cusumano *et al.* [8, 9] studied the correlation between the 99% criterion and the false nearest neighbours test for dimensionality of the reconstructed phase space. The validity of the 99% criterion in the selection of dominant modes is verified as follows. In Figure 4 the phase portraits (plots of velocity versus displacement of the driven mass) of different reduced models of the system with different levels of reduction are shown. Note that for the system under consideration, six of the modes have eigenvalues summing up to 99% of the total. The one and two mode reduced model phase portraits have not been shown as they deviate well beyond the range shown in the figure.

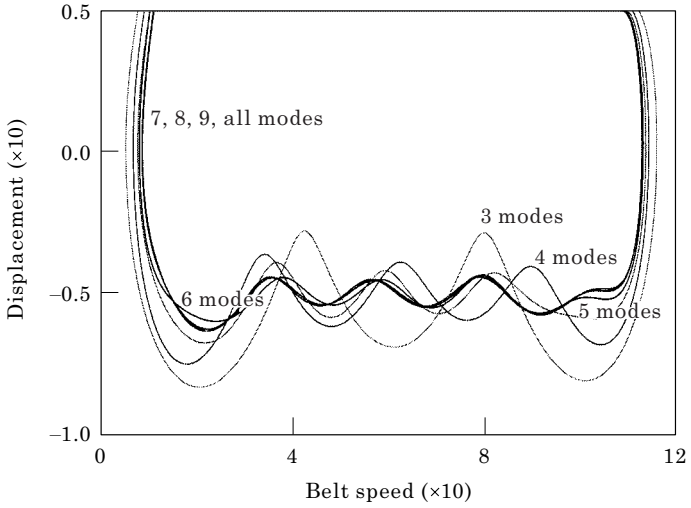

Figure 4. Phase portraits of 10-SMD system, with different levels of reduction. A qualitative comparison for determining the order of reduction.

For quantitative comparison of the full and reduced systems two different measures were considered. One of the measures corresponds in a sense to the total energy in the system. The energy E in the system can be represented by

$$E = \tfrac{1}{2}\sum_{i=1}^{M} \dot{X}_i^2 + \tfrac{1}{2}X_i^2 + \tfrac{1}{2}\sum_{i=2}^{M}(X_i - X_{i-1})^2. \tag{18}$$

With this relation one can define $\mathbf{E}_f$ and $\mathbf{E}_r$ for the energies in the full and reduced system respectively. The deviation of the reduced system from the full system can then be represented by

$$\Delta E = 100\ \frac{(\mathbf{E}_f - \mathbf{E}_r)}{\mathbf{E}_f} \tag{19}$$

and this deviation is used as one of the measures.

Other measures that one uses to compare are the deviations in the displacements and velocities of the individual masses and the sum square of those deviations:

$$\Delta X = 100\sqrt{\left(\sum_{i=1}^{M} \Delta X_i^2 + \Delta \dot{X}_i^2\right) \Big/ \left(\sum_{i=1}^{M} X_i^2 + \dot{X}_i^2\right)}. \tag{20}$$

This measure would take care of the problems where one has the first measure small in spite of a large phase difference. Table 1 shows the statistical measures of deviation of the models from the full model.

From the qualitative comparison one finds that with six-mode reduction the orbit is close to that of the full system. From the table one also notes that the statistical deviation of the reduced system from the full system is well within the limits. As such the 99% criterion is accepted for selection of number of modes and one continues with the research. One however must mention that for some engineering applications, agreement such as the three-mode case is considered great and settling for two or three-mode cases considerably simplifies the analysis of the system.

TABLE 1

Statistical deviations at different levels of reduction

No. of modes (L)	9	8	7	6	5	4	3
$\sum_{i=1}^{L}\lambda_i \Big/ \sum_{i=1}^{M}\lambda_i \times 100$	99·99	99·95	99·90	99·59	98·53	96·50	94·05
ΔX	0·05	0·25	0·39	1·08	2·17	4·67	6·07
ΔE	0·01	0·02	0·01	0·06	0·44	0·99	2·07

6. VALIDATION OF REDUCED MODEL

Now that the order of reduction has been decided, the next step is to validate the reduced model. Different methods have been considered in comparing two non-linear systems. The foremost method is to compare the qualitative behavior of the two systems. The next is to look at the energy content. This gives a quantitative comparison. Another important feature of non-linear systems is the occurrence of bifurcations and jumps. Towards this one compares the bifurcation diagrams generated from the two systems. The chaotic dynamics can be compared using Lyapunov exponents. Another comparison for chaotic dynamics is the comparison of skeletons of the attractors.

6.1. QUALITATIVE COMPARISON

For qualitative comparison one refers to Figure 5, where the phase portraits of the system obtained from the full and reduced models are depicted. Phase portraits of the system are obtained by plotting the displacement versus velocity of the driving mass. With different initial conditions and belt speeds the system gives rise to different dynamics and the corresponding phase portraits are plotted from the reduced and full models. In the plots are shown the phase portraits from the reduced model in the top row and those from the full model in the bottom row.

One can observe that the phase portraits of the two systems look similar, including the complicated orbits of higher periods, where although there are deviations, the size of the attractor is of the same order.

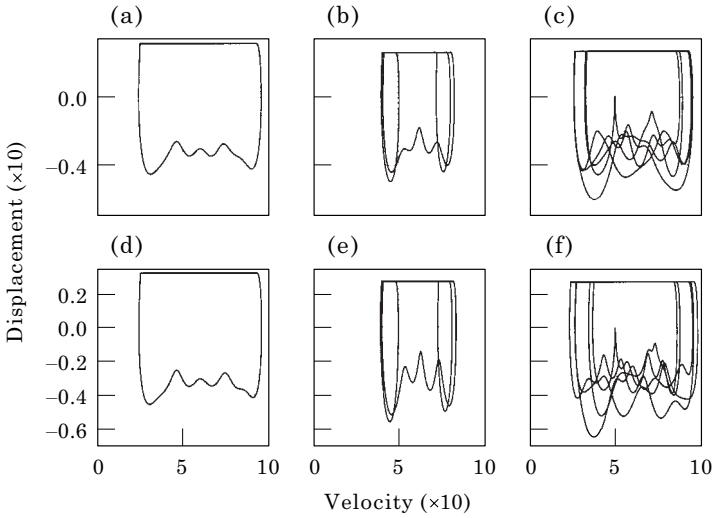

Figure 5. Qualitative comparison between full and reduced models. Top row (a), (b) and (c) correspond to the dynamics of the reduced model and bottom row (d), (e) and (f) to the full model. Each column corresponds to a set of identical initial conditions. All other parameters are kept constant.

TABLE 2

Quantitative comparison between full and reduced models; Δx and ΔE are defined in equations (20) *and* (19) *respectively*

Period	ΔX (%)	ΔE (%)
1	0·614	0·095
3	2·527	1·350
5	4·873	0·610

6.2. QUANTITATIVE COMPARISON

For quantitative comparison of the periodic orbits, one can use the same measures that were used in determining the order of reduction. In Table 2 these measures are listed for the three periodic orbits that were used for qualitative comparison. From Table 2 one realizes that the statistical deviations of the reduced model predictions from the full model predictions are rather small, more so from the energy perspective. One does not want to elaborate on this comparison as the tolerances allowed are application dependent. For example, in a computer assembly plant the tolerances could be fractional percentages whereas in a steel plant even 5–6 percent deviation is considered acceptable. One also notes that in some applications the maximum deviation between the predicted and actual displacements of the system at some particular location would be the deciding factor. An example would be the case of a pick-and-place robot manipulator. The allowable deviation is again dependent on the specific application.

6.3. COMPARISON OF BIFURCATIONS

Another possible method of comparing the two systems is to check for the occurrence of bifurcations. Towards this goal the bifurcation diagrams (Figure 6) for both of the models were generated and a comparison made. One varied the belt speed from 0·500–0·001 in steps of 0·001. The initial conditions at each belt speed equal the end conditions of the previous speed for the reduced system. Note that the same initial conditions that were used for the reduced model at each belt speed have been used for the full model also. Thus one is comparing the system dynamics in steady state that go close to the subspace spanned by the L modes of the system. Here one presents the two bifurcation diagrams.

As typical of any two non-linear systems, one sees differences. The difference is small when the reduced system predicts periodic orbits. However, for bifurcations into non-periodic orbits, the predictions did not match well with the full model. This could be attributed to a shift in basin boundary and the sensitive dependence on the initial conditions of the chaotic systems.

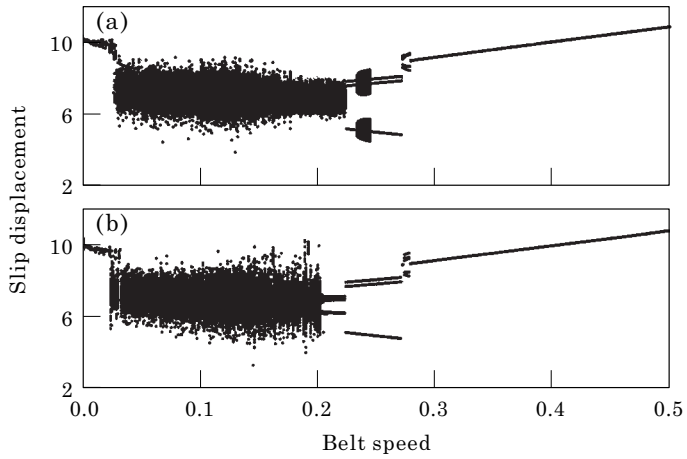

Figure 6. Comparison between (a) reduced and (b) full models: bifurcations.

6.4. UNSTABLE PERIODIC ORBITS

During a chaotic orbit, the system visits countably many unstable periodic orbits, see reference [23]. These unstable periodic orbits form the skeleton of the chaotic orbit. One way of comparing the chaotic orbits is to compare these skeletons. Lathrop [23] gives a procedure of extracting the unstable periodic orbits in a reconstructed attractor from a time series. In this method a phase–space attractor is reconstructed from the data using the standard method of time delays. The attractor is the set of points $y(n) = (s_n, s_{n+T}, \cdots s_{n+(d-1)T})$. The time delay T and embedding dimension d are determined as earlier on the basis of mutual information and false nearest neighbors respectively. The orbits are located as follows. Let $\varepsilon > 0$, and let $y(i)$ be a point on the reconstructed attractor. One follows the observed images $y(i + 1)$, $y(i + 2)$, $\cdots$ of $y(i)$ until one finds the smallest index $k > i$ such that $||y(k) - y(i)|| < \varepsilon$. If such a k exists, one defines $m = k - i$ and say that $y(i)$ is an (m, ε) recurrent point.

In this analysis one fixes $\varepsilon = 0{\cdot}5 \times \Delta y$, where Δy is the average distance between two consecutive points on the attractor. In the following one shows the skeletons of the attractors (Figure 7) reconstructed from the velocity time series of the first mass, obtained during the sweeps when the belt speed is 0·2, both the systems starting with identical initial conditions. One finds that the approximate unstable orbits have close resemblances qualitatively.

7. DISCUSSIONS AND CONCLUSIONS

Proper orthogonal decomposition has been used in a Galerkin-based order reduction of a frictionally excited multi-degree-of-freedom numerical system. This work thus bridges the work of Cusumano and Bai [8] which relates the size of a non-smooth system to spatial coherence of the system and the work of FitzSimons [10] which deals with modal reduction of simple smooth systems

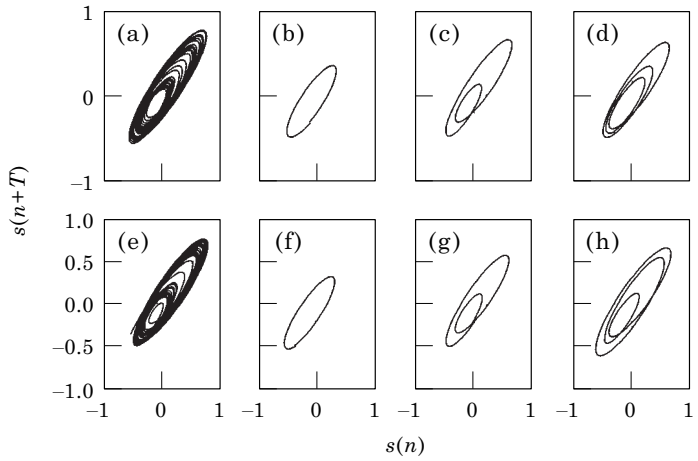

Figure 7. Unstable periodic orbits in the chaotic attractor reconstructed from the velocity time series of the first mass. The first row (a), (b), (c) and (d) corresponds to data from the reduced model and the second row (e), (f), (g) and (h) to data from the full model. The first column (a) and (e) shows part of the attractor. The remaining shows approximate unstable periodic orbits of periods 1—(b) and (f), 2—(c) and (g) and 3—(d) and (h).

using POD. Also in this paper modal reduction and modal projection in a stick–slip system were reinforced, which is a non-trivial task.

Though the reduction is only from an order 20 to an order 12 (this being a discrete system), one suspects a better reduction can be achieved for the same criterion, in the case of continuous systems where only a few modes of the system dominate the dynamics. Another important issue is that the criterion used for picking the number of modes is application dependent, the same criterion can be better for some applications and can be worse for some others. Detailed analysis of an experimental system with frictional excitation is presented in another paper where a beam subjected to frictional excitation at the tip is modelled and is described by three dominant POMs. The reduction in the order helps in applications like building controls, viz. the control of robot manipulators where non-smooth forcing like friction and impact are imperative.

ACKNOWLEDGMENTS

We acknowledge NSF for funding (CMS-9624347) and Professors Charles MacCluer, Steve Shaw, Alan Haddow and Clarke Radcliffe for valuable comments.

REFERENCES

1. J. L. LUMLEY 1970 *Stochastic Tools in Turbulence*. New York: Academic Press.
2. D. KOSAMBI 1943 *Journal of Indian Mathematical Society* **7**, 76–88, Statistics in function space.
3. M. LOEVE 1963 *Probability Theory*. Princeton, NJ: Van Nostrand.

4. K. KARHUNEN 1956 *Annu. Acad. Sci. Fennicae* A, 1–34. Zur Spektral Theorie Stochastischer Prozesse.
5. V. S. POUGACHEV 1953 *Izv. Akad. Nauk. SSSR* **17**, 1401–1402. General theory of correlations of random functions.
6. B. RAVINDRA 1998 *Journal of Sound and Vibration (to appear)*, On the physical interpretation of proper orthogonal modes in vibrations.
7. G. BERKOOZ, P. HOLMES and J. L. LUMLEY 1993 *Annual Review of Fluid Mechanics* **25**. New York: Annual Reviews Inc. The proper orthogonal decomposition in the analysis of turbulent flows.
8. J. P. CUSUMANO and B. Y. BAI 1993 *Chaos, Solitons and Fractals* **3**, 515–535. Period-infinity periodic motions, chaos and spatial coherence in a 10-degree-of-freedom impact oscillator.
9. J. P. CUSUMANO, M. T. SHARKADY and B. W. KIMBLE 1994 *Philosophical Transactions of Royal Society of London*. Experimental measurements of dimensionality and spatial coherence in the dynamics of a flexible-beam impact oscillator.
10. P. FITZSIMONS and C. RUI 1993 *Advances in Robust and Nonlinear Control Systems*, ASME DSC-Vol. **53**. Determining low dimensional models of distributed systems.
11. K. D. MURPHY 1996 *Proceedings of the sixth Conference on Nonlinear Vibrations, Stability and Dynamics of Structures*, June, Virginia. Using the Karhunen-Loeve decomposition to examine chaotic snap-through oscillations of a buckled plate.
12. F. BESSAC, L. GAGLIARDINI and J. L. GUYADER 1996 *Journal of Sound and Vibration* **191**, 881–899. Coupling eigenvalues and eigenvectors: a tool for investigating the vibroacoustic behavior of coupled vibrating systems.
13. S. R. SIPCIC and A. BENGUEDOUAR and A. PECORE 1996 *Proceedings of the sixth Conference on Nonlinear Vibrations, Stability and Dynamics of Structures*, June, Virginia. Karhunen-Loeve decomposition in dynamical modeling.
14. B. FEENY and R. KAPPAGANTU 1998 *Journal of Sound and Vibration* **211**, 607–616. On the physical interpretation of proper orthogonal modes in vibrations.
15. M. A. DAVIES and F. C. MOON 1997 *Nonlinear Dynamics: The Richard Rand* 50*th Anniversary Volume*. Singapore: World Scientific.
16. X. MA, M. A. F. AZEEZ and A. VAKAKIZ 1998 *Proceedings of the seventh Conference on Nonlinear Vibrations, Stability and Dynamics of Structures*, Blacksburg. Nonparametric nonlinear system identification of a nonlinear flexible system using proper orthogonal mode decomposition.
17. T. SUGIMOTO 1984 *Automotive Technology* **35**. Stick–slip friction.
18. W. E. WHITEMAN and A. A. FERRI 1997 *Journal of Sound and Vibration* **207**, 403–418. Multimode analysis of beam-like structures subjected to displacement dependent dry friction.
19. A. WOLF, J. B. SWIFT, H. L. SWINNEY and J. A. VASTANO 1985 *Physica D* **16**, 285–317. Determining Lyapunov exponents from a time series.
20. A. M. FRASER and H. L. SWINNEY 1986 *Physical Review*. Information and entropy in strange attractors.
21. A. M. FRASER 1989 *Physica D* **34**, 391–404. Reconstructing attractors from scalar time series: a comparison of singular system and redundancy criteria.
22. M. B. KENNEL, R. BROWN and H. D. I. ABARBANEL 1992 *Physics Letters A* **45**, 3403–3411. Determining embedding dimension for phase-space reconstruction using a geometrical construction.
23. D. P. LATHROP and E. J. KOSTELICH 1989 *Physical Review A* **40**, 4028–4031. Characterization of an experimental strange attractor by periodic orbits.